

Prefer-DAS: Learning from Local Preferences and Sparse Prompts for Domain Adaptive Segmentation of Electron Microscopy

Jiabao Chen, Shan Xiong, and Jialin Peng

Abstract—Domain adaptive segmentation (DAS) is a promising paradigm for delineating intracellular structures from various large-scale electron microscopy (EM) without incurring extensive annotated data in each domain. However, the prevalent unsupervised domain adaptation (UDA) strategies often demonstrate limited and biased performance, which hinders their practical applications. In this study, we explore sparse points and local human preferences as weak labels in the target domain, thereby presenting a more realistic yet annotation-efficient setting. Specifically, we develop Prefer-DAS, which pioneers sparse promptable learning and local preference alignment. The Prefer-DAS is a promptable multitask model that integrates self-training and prompt-guided contrastive learning. Unlike SAM-like methods, the Prefer-DAS allows for the use of full, partial, and even no point prompts during both training and inference stages and thus enables interactive segmentation. Instead of using image-level human preference alignment for segmentation, we introduce Local direct Preference Optimization (LPO) and sparse LPO (SLPO), plug-and-play solutions for alignment with spatially varying human feedback or sparse feedback. To address potential missing feedback, we also introduce Unsupervised Preference Optimization (UPO), which leverages self-learned preferences. As a result, the Prefer-DAS model can effectively perform both weakly-supervised and unsupervised DAS, depending on the availability of points and human preferences. Comprehensive experiments on four challenging DAS tasks demonstrate that our model outperforms SAM-like methods as well as unsupervised and weakly-supervised DAS methods in both automatic and interactive segmentation modes, highlighting strong generalizability and flexibility. Additionally, the performance of our model is very close to or even exceeds that of supervised models.

Index Terms—Domain Adaptive Segmentation, Electron Microscopy, Local Preference Learning, Promptable Segmentation, Sparse Points

I. INTRODUCTION

AS transmission electron microscopes (TEM) and scanning electron microscopes (SEM) rapidly develop, high-resolution volume electron microscopy (EM) images are becoming indispensable in biomedical research, experimental pathology, and diagnostic pathology for investigating intracellular structures and various diseases [1]. A crucial initial step for analyzing intracellular structures across different cell types and states of cellular health using EM images is the precise and efficient segmentation of objects of interest, such as mitochondria, within diverse cellular contexts. Recently, deep neural networks, including convolutional neural networks

This work was partly supported by the National Natural Science Foundation of China under Grant 12471498 and the Natural Science Foundation of Xiamen under Grant 3502Z202373042. (Corresponding author: Jialin Peng)

J. Chen and S. Xiong are with College of Computer Science and Technology, Huaqiao University, Xiamen 361021, China.

J. Peng is with College of Computer Science and Technology, Huaqiao University, Xiamen 361021, China (e-mail: jialinpeng@hqu.edu.cn).

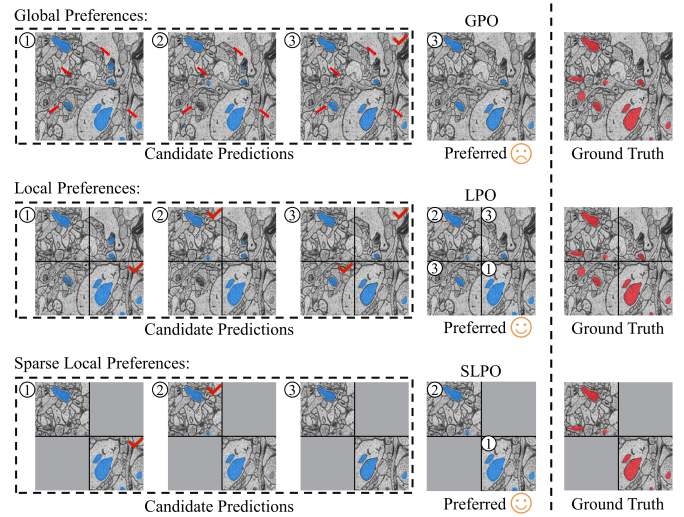


Fig. 1. A visualization of the concept of local human preferences and sparse local preferences. While selecting the preferred segmentation at the image level usually poses challenges for human raters and results in misleading signals, we gather local preferences at the patch level. In practical use, requiring sparse local preferences on only a few key patches is more convenient and annotation-efficient. Here, 2×2 patches are used solely for illustrative purposes.

[2] and vision transformers (ViTs) [3] have revolutionized the field of automatic image segmentation [4]–[8]. However, developing deep learning approaches presents significant challenges, as the amount of labeled data available and the granularity of annotation for training have a profound impact on the model performance and generalization capabilities. For EM images, manual annotation of numerous instances of morphologically complex organelles requires substantial costs and expert knowledge. Moreover, deep learning models are sensitive to the variability in distributions, which is typically observed across different EM images due to differences in microscopy techniques, imaging protocols, and the inherent diversity of cell types.

Domain adaptive segmentation (DAS) focuses on adapting well-trained models from related domains (source domain) to the target domain, thereby presenting a promising strategy for reducing the necessity of annotating extensive datasets for each new domain. To alleviate the issues associated with the distribution shift or domain shift, various DAS approaches have been introduced. A prevalent setting is Unsupervised Domain Adaptation (UDA), which operates under the assumption that source data is fully labeled while the target data remains unlabeled. However, in the absence of label information for the target data, UDA methods frequently encounter difficulties

in achieving satisfactory performance, particularly in complex tasks. Although Semi-supervised Domain Adaptation (SDA) can achieve boosted performance with sufficient pixel-wise labels on the target domain, it demands substantial annotation effort.

To mitigate these challenges, we propose leveraging weak labels on the target domain and conducting Weakly Supervised Domain Adaptation (WSDA), thereby significantly reducing annotation costs and the need for strong expert knowledge while achieving competitive performance. In this study, we consider two forms of weak supervision for model training: 1) Type I: sparse center point annotation, which is particularly aligned with EM image segmentation or other cell image segmentation; 2) Type II: sparse patch-level preference annotation, which is the rating information of the segmentation on partial patches and is suitable for general segmentation tasks. Importantly, compared to fully annotating all center points for each object instance in EM images, randomly annotating sparse points on a small number of object instances requires fewer expert resources and can usually be easily completed by non-experts.

Recently, there has been a shift towards developing more flexible, user-oriented segmentation paradigms, such as promptable and interactive models, aiming to enhance segmentation performance by incorporating human knowledge and feedback during either the training stage or the inference stage. Particularly, prompt-driven foundation models have shown remarkably strong generalization abilities without training on specific targets. For instance, the large-scale segmentation model SAM [9], which is pre-trained on billion-scale datasets of natural images, has demonstrated impressive performance on various segmentation tasks. The SAM treats human interactions, such as points, boxes, or masks, as prompts to guide segmentation during both the training and inference stages. The promptable segmentation models pave the way for the longstanding interactive segmentation, which can be responsive to user intention or progressively refine the segmentation. However, SAM relies on prompting for each instance to segment all object instances, making it particularly challenging to segment numerous organelle instances from EM images. SAM still struggles with domain shifts and usually shows low performance on medical image tasks, especially with point prompts, due to the lack of medical knowledge, ambiguous boundaries, and complex shapes. To enhance the performance, several studies [10]–[12], have proposed modifying or fine-tuning SAM using medical data, such as SAM-Med2D [11], Med-SA [12]. Furthermore, SAM, like other supervised models, just learns from paired image-annotation datasets and does not incorporate human feedback throughout the training process.

Rather than relying on prompts, another line of research biases the trained model to human intentions through post-processing techniques. For Large Language Models (LLMs), strategies such as Reinforcement Learning from Human Feedback (RLHF) [13] and Direct Preference Optimization (DPO) [14] have been widely used to learn from human preferences. Unlike RLHF, the DPO strategy refines LLMs directly by utilizing human preferences, without relying on explicit reward

modeling. Recently, DPO has also been applied in visual tasks, such as integrating with diffusion models for generating physically plausible images [15], [16]. However, human preference alignment for image segmentation with DPO remains largely underexplored. Unlike signals and language sentences, images convey complex spatial information. The quality of segmentation within an image by a model is typically suboptimal, with inaccurate boundaries or even partial locations. Exploring human ratings as preferences is an annotation-efficient way to enhance the initial segmentation model. However, the quality of a segmentation prediction within an image often varies across different areas. As a result, evaluating the segmentation quality of an entire image—particularly in cellular images like electron microscopy (EM) images—can be cumbersome and less meaningful. Since typical UDA and WDA suffer from imprecise segmentation and segmentation bias, we propose enhancing our initially trained segmentation model with novel *local preference learning* in an annotation-efficient manner.

In this study, we introduce Prefer-DAS, a preference-guided promptable transformer model for domain-adaptive segmentation of EM images, using weak supervision. As a preference-guided model, we draw upon human ratings of the relative quality of different segmentation predictions to guide our model training and control of the behavior of our segmentation model. The proposed preference learning module is formed as a plug and play that can be combined with UDA and WDA. Since it is usually challenging to select the best prediction for an image from a set of suboptimal segmentations, we propose using local ratings instead of global preferences for preference learning. As shown in Fig. 1, conducting local ratings is more intuitive and user-friendly for human annotators, requiring significantly less annotation effort. To further decrease annotation cost, we also explore sparse local preferences and self-learned ratings.

As a prompt-driven model, our Prefer-DAS is flexible and can effectively utilize both full and partial prompts during the training and testing phases, enabling it to conduct both standard segmentation and interactive segmentation. To minimize the annotation burden, we utilize sparse points as cost-effective prompts for the semantic segmentation of all object instances within the EM images. Unlike SAM-based models, which require training on billion-scale datasets, we adapt a model trained on a source domain from scratch to a new target domain that already has sparse points available for the target training data and does not assume the availability of prompts during the testing stage. However, when point prompts are available during the testing stage, the output of our method can further align with user intent. Moreover, our model conducts one-pass segmentation of many object instances with any point prompts, presenting an advantage over SAM. To enhance discriminative feature learning, we introduce a novel prompt-guided contrastive learning. Comprehensive experiments conducted on challenging benchmarks demonstrate the effectiveness of the proposed approach.

A preliminary conference version of this study appears in [17], in which we introduced the Prompt-DAS model. This improved version introduces preference learning and (sparse) local preferences as forms of weak supervision and takes

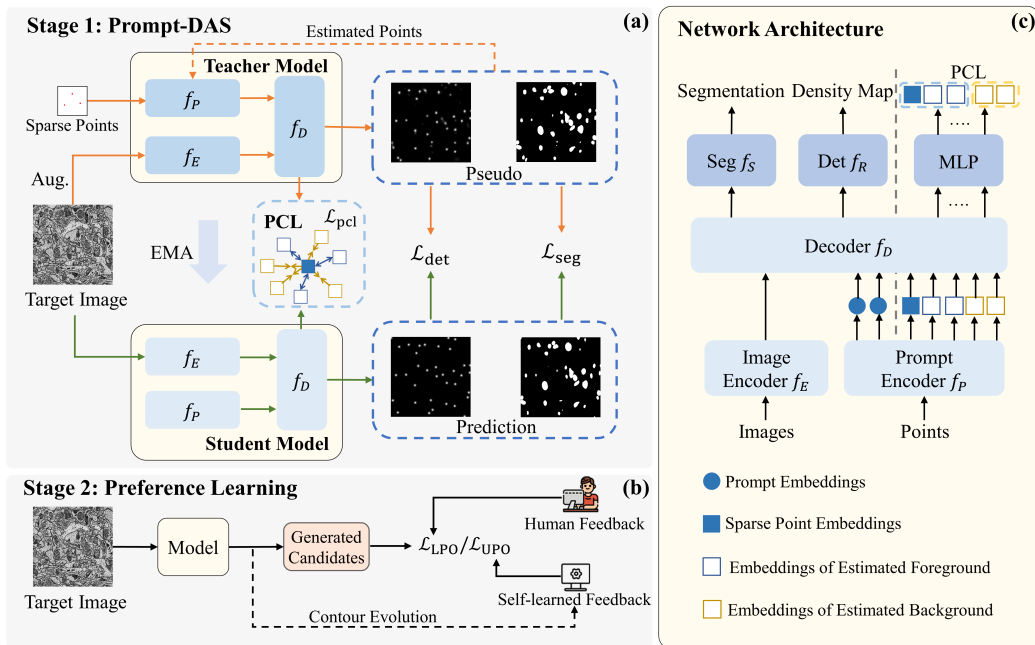


Fig. 2. Overall framework of the proposed Prefer-DAS model for weakly-supervised domain adaptive segmentation. Our framework comprises two stages. The first stage performs promptable domain-adaptive segmentation for UDA or WDA segmentation, depending on the availability of sparse points; the second stage performs locally supervised or unsupervised preference learning, depending on the availability of human preferences.

advantage of both prompt learning and preference learning. The Prefer-DAS model demonstrates significantly stronger performance than the Prompt-DAS model on more domain adaptation tasks.

II. RELATED WORK

A. Domain Adaptive Segmentation

Most machine methods experience degraded performance when there is a discrepancy between the distributions of training and testing data. This decline in performance is also evident in cutting-edge large-scale models, such as the foundation segmentation model SAM [9]. While SAM demonstrates strong zero-shot generalization ability on various natural images with human prompts, it suffers significant performance drops on biomedical datasets [18], including electron microscopy (EM) images. Although several medical variants of SAM, such as SAM-Med2D [11], Med-SAM Adapter [12], have been introduced, they still suffer from the large domain gaps among medical data.

Most domain adaptation methods tackle domain adaptive segmentation by aligning the source and target distributions in various spaces: input image space [19], latent feature space [20], output space [21], or through a combination of these approaches [4]. Recently, self-training, which focuses on exploiting unlabeled target data by estimating pseudo labels, has become a popular gain to existing adaptation methods due to its simple concept. For mitochondria segmentation from EM images, the 2D model DAMT-Net [4] jointly learns domain-invariant visual and geometrical features using adversarial learning and an autoencoder. The DA-ISC [5] is a 2.5D method that integrates output-space adversarial learning with

a novel intersection consistency technique. The UALR method [5] is a self-training-based method that rectifies noisy labels by estimating their uncertainty. Furthermore, the CAFA [7] method enhances self-training through class-aware feature alignment. Additionally, our previous work, WDA-Net [22] also conducts WDA segmentation using novel sparse points as the weak supervision. Despite the significant advances in UDA and WDA tasks, prior methods typically can not accept human feedback and interaction and suffer from imprecise segmentation and model-biased segmentation. Our current work introduces the first local preference-guided WDA model, which can also utilize sparse point prompts as the WDA-Net [22].

B. Learning with Visual Prompts

Beyond automatic segmentation, a longstanding research direction is to develop models that can leverage user interaction, which is particularly beneficial for medical image analysis. The SAM model [9], which was pretrained on 1 billion masks on 11 million natural images, conducts interactive segmentation by using user-provided bounding boxes, points, and masks as inference prompts, showing remarkable performance across various zero-shot tasks. Typically, SAM's effectiveness is influenced by the type of prompts [18] and is sensitive to the randomness associated with point and box prompts. Generally, the performance of SAM with point prompts is not as strong as with box prompts. A significant limitation of the SAM model is that it requires at least one prompt for each object instance, which can complicate the segmentation of images that contain a large number of objects, such as cellular images. In this study, we introduce a promptable model that allows for

inference with full, partial, or no point prompts for all target predictions in a single pass.

C. Learning from Human Preferences

Reinforcement Learning from Human Feedback (RLHF) is currently the predominant paradigm for aligning foundation models with human preferences. However, it is limited by its reliance on learning an additional reward model to represent human preferences. A promising alternative is Direct Preference Optimization (DPO) [14], which streamlines the process by directly optimizing the policy model using human preference data, eliminating the necessity for iterative reinforcement learning training. DPO typically employs pairwise user preferences, consisting of one human-preferred prediction and one less-preferred prediction (single negatives), along with the Bradley-Terry model [23] for preference distribution modeling. To avoid the oversight of other negative items, the Softmax-DPO [24] use Plackett-Luce model [25] for preference distribution modeling, allowing the pairing of a preferred prediction with multiple less-preferred predictions (multiple negatives).

Various DPOs have shown notable success when integrated with large language models (LLMs), large vision-language models (LVLMs), and diffusion models. The POPEN model [26] leveraged feature-similarity-based DPO to reduce hallucinations in LVLM-based reasoning segmentation with text input. Konwer *et al.* [27] improved SAM with DPO for semi-supervised segmentation of medical images, in which global ratings on the quality of candidate segmentation are used. While globally rating and ranking the quality of two or more segmentation predictions is challenging and often less meaningful, we explore local and sparse preference learning, allow us to efficiently fine-tune our segmentation models using limited preference data. To further reduce the annotation effort, we also introduce self-learned preferences, as the proximity to human preferences, and develop an unsupervised DPO.

III. PRELIMINARIES

Direct Preference Optimization. Preference alignment has demonstrated to be effective in enhancing LLMs. Without using a learned reward model as RLHF, the standard DPO maximizes the generation probabilities of the paired human preference data $\mathcal{D}_h = \{(x, y_p, y_d)\}$, where y_p is preferred by the human rater over y_d . Based on the Bradley-Terry model [23], the probability that the prediction y_p is preferred over the prediction y_d for the image x is modeled as:

$$P(y_p \succ y_d|x) = \sigma\left(r(x, y_p) - r(x, y_d)\right) \quad (1)$$

where $r(\cdot, \cdot)$ is the reward model that measures how well a prediction y meets human preference for the given input x . While RLHF conducts a two-stage learning process with explicit reward modeling and policy optimization, the DPO directly optimizes the policy based on the connection between the reward and the optimal RLHF policy $p_\theta^*(y|x)$.

$$r(x, y) = \beta \log \frac{p_\theta^*(y|x)}{p_{\theta_0}(y|x)} + \beta \log Z(x) \quad (2)$$

where $Z(\cdot)$ is the unknown partition function, and p_{θ_0} is the reference policy parameterized by θ_0 . Given the preference probability model, the standard DPO learns the optimal policy by minimizing the negative log-likelihood loss,

$$\mathcal{L}_{\text{DPO}}^{BT} = -\mathbb{E}_{\mathcal{D}_h} \left[\log \sigma \left(\beta \log \frac{p_\theta(y_p|x)}{p_0(y_p|x)} - \beta \log \frac{p_\theta(y_d|x)}{p_0(y_d|x)} \right) \right] \quad (3)$$

When multiple negatives is paired with the preferred prediction, we can derive similar expressions under the Plackett-Luce models [24], [25],

$$\mathcal{L}_{\text{DPO}}^{PL} = -\mathbb{E}_{\mathcal{D}_h} \left[\log \sigma \left(-\log \sum_{j=1}^{J-1} \exp \left(\beta \log \frac{p_\theta(y_p^j|x^l)}{p_0(y_p^j|x^l)} - \beta \log \frac{p_\theta(y_{d_j}^l|x^l)}{p_0(y_{d_j}^l|x^l)} \right) \right) \right] \quad (4)$$

IV. METHOD

A. Overview

1) *Problem Setting:* This study investigates cross-domain segmentation of mitochondria from EM images under weak supervision. Specifically, we have a well-trained model on the source domain $\mathcal{D}^s = \{(x^s, y^s)\}$, which has full pixel-wise labels y^s , and a weakly-labeled target domain $\mathcal{D}^t = \{(x^t, w^t)\}$ with weak labels w^t . In addition to the *sparse point labels* $w^t = \bar{c}^t$ used in our preliminary version [17], we further introduce one time human feedback on the training data, i.e., human preferences on different segmentation predictions, as the weak supervision in the form of *local preferences* $w^t = r^t$ and *sparse local preferences* $w^t = \bar{r}^t$. Rather than obtaining the preferred segmentation by globally evaluating candidate segmentation predictions $\{y_i^t\}_{i=1}^K$, as illustrated in Fig. 1, the local preference setting selects the preferred segmentation y_p^t and dispreferred ones $\{y_d^t\}$ in a patch-wise way. For sparse local preferences, a human evaluator only needs to assess the segmentation quality on a small proportion (by default, 15%) of patches to obtain a sparsely preferred segmentation \bar{y}_p^t and sparsely dispreferred ones $\{\bar{y}_d^t\}$. In addition, we also devise *simulated preferences* $w^t = \bar{r}_s^t$ as self-learned weak labels.

Our objective is to develop a model that is flexible enough to perform UDA, WDA, as well as interactive versions of UDA and WDA depending on the availability of human prompts. The model should also be flexible enough to be capable of effectively utilizing both human prompts and preferences when provided.

2) *Model Overview:* Figure 2 illustrates the proposed Prefer-DAS, which encompasses an image encoder f_E , a point prompt encoder f_P that processes $M \geq 0$ points at once as inputs, a multitask decoder f_D followed by a semantic segmentation head f_S , and a regression-based center-point detection head f_R . Additionally, the model includes a preference calibration module. By default, our Prefer-DAS model utilize 15% sparse points as training prompts, and local human preferences for preference learning. In scenarios where NO human preferences are available during model training, our Prefer-DAS model reverts to our preliminary version,

Prompt-DAS. Furthermore, when partial/full point prompts are provided during the testing phase, our model performs interactive segmentation, denoted as Prefer-DAS+.

To address the issue of label scarcity on the target domain during domain adaptation learning, we conduct pseudo-label learning for both the segmentation and detection tasks under the mean-teacher framework [28]. The output of the detection head f_R is used to provide prompts for the segmentation task. Furthermore, the segmentation head f_S is guided by a prompt-based contrastive loss, enhancing the discriminability of prompt embeddings.

B. Promptable Detection

The proposed Prefer-DAS utilizes an auxiliary detection task to enhance the segmentation learning. The center point detection task is relatively easier than the dense segmentation task, particularly given sparse points as training prompts and partial supervision. While the joint learning of multiple tasks can implicitly boost the segmentation performance, confident detection outputs are further employed to augment the ground-truth point prompts for the segmentation task. Following the teacher-student framework [28], pseudo-labels for the unlabeled regions are generated by selecting most highest local maxima points with a threshold from the predicted density map by the teacher model, which is updated by the exponential moving average of the student network. Note that local maxima points can be identified through Non-Maxima Suppression. For the target data, student network training is supervised by both the ground-truth sparse points and pseudo labels, and the M sparse points are also used as training prompts. In the scenario of UDA, where there are no point annotations on the target domain, we use the estimated confident points from the prediction of the source model as the pseudo-sparse points. For the source data, ground truth center points are used as the supervision, and randomly sampled n_s center points are used as training prompts.

$$\mathcal{L}_{\text{det}} = \frac{1}{|D^s|} \sum_{x^s} L_d(F_R(x^s), d^s) + \frac{1}{|D^t|} \sum_{x^t} L_d(F_R(x^t), \hat{d}^t) \quad (5)$$

where $F_R = f_R \circ f_D \circ f_E$, L_d represents mean square error loss, and \hat{d}^t represents the density map generated by the target pseudo labels and ground truth points.

C. Promptable Segmentation

To alleviate label scarcity, we leverage pseudo-labeling in the teacher-student framework. Thus, both ground truth source labels and target pseudo-labels are used to supervise the model training.

$$\mathcal{L}_{\text{seg}} = \frac{1}{|D^s|} \sum_{x^s} L_s(F_S(x^s), y^s) + \frac{1}{|D^t|} \sum_{x^t} L_s(F_S(x^t), \hat{y}^t) \quad (6)$$

where $F_S = f_S \circ f_D \circ f_E$, L_s represents the standard cross-entropy loss, \hat{y}^t represents the pseudo labels generated by the teacher model on the target domain.

Similar to the detection head, we also use points as the segmentation training prompts. For the source domain, we use

the n_s points sampled for the detection task as the training prompts. Note that n_s is a random number during training. Since the target data only has a few points as the annotation, we propose to use both the estimated points from the detection output and ground-truth sparse points as training prompts to assist the segmentation training. The target point prompts are generated by selecting most highest local maxima points with a threshold from the predicted density map by the detection head.

D. Prompt-guided Contrastive Learning (PCL)

To learn more discriminative embeddings during pseudo-label learning, we further introduce contrastive learning with the guidance of prompts, which can provide representative features to distinguish mitochondria instances from the background organelle. As shown in the left figure of Fig. 2, our contrastive learning aims to pull the feature embeddings of the estimated foreground points closer to those of the ground-truth sparse points while simultaneously pushing away from the foreground embeddings from the background embeddings. An MLP layer ϕ is utilized before conducting contrastive learning. Let $z^t = \phi(f_D(f_P(p^t)))$ denote the embedding derived from the target domain point p^t . We employ an attention mask mechanism following DN-DETR [29] to prevent information leakage from PCL.

Queries are generated from pixels identified as foreground exhibiting a sufficiently high confidence. Utilizing the pseudo-labels produced by the teacher model, we select 3 points from each instance with a confidence greater than δ_f , resulting in N^q foreground prompt embeddings $\{z_i^t\}_{i=1}^{N^q}$. Concurrently, we identify N^n points with a confidence level below δ_b , resulting in N^n background prompt embeddings $\{\mu_k^b\}_{k=1}^{N^n}$. Since mitochondrial instances display high similarity, we employ the average embedding of sparse point prompts as the sparse prompt embedding μ^f . The prompt-guided contrastive loss is defined as follows:

$$\mathcal{L}_{\text{pcl}} = - \sum_{i=1}^{N^q} \log \left[\frac{\exp(\mu^f \cdot z_i^t / \tau)}{\exp(\mu^f \cdot z_i^t / \tau) + \sum_{k=1}^{N^n} \exp(\mu_k^b \cdot z_i^t / \tau)} \right] \quad (7)$$

E. Local Preference Learning

Typically, the predictions of a segmentation model is usually biased by the modeling techniques in use and the data itself, and this issue is more severe due to the domain gap, domain-adaptive segmentation method, and the available labeling information on the target domain. To address these issues with low annotation cost, we propose aligning the segmentation model with human ratings through preference learning. Our objective is to ensure that our segmentation model generates segmentation predictions preferred by human raters with a higher probability than segmentation predictions that are not preferred. More specifically, we fine-tune an initially trained model on human-labeled reference data with improved DPO strategies. Thus, our strategy is a plug-and-play method that is model-agnostic.

1) **Local direct Preference Optimization (LPO)**: Given several candidate segmentation predictions, a significant challenge in constructing human preference data is selecting the best segmentation prediction. Images contain spatial information and often contain complex contents. Typically, a segmentation may perform better than other segmentation in certain local regions but worse in other local regions. Thus, it is usually prohibitive to directly select the preferred segmentation from candidate segmentation predictions of low quality. To address these issues, we first introduce the LPO for the segmentation task. Specifically, we split each input image x and its predictions into $L \times L$ patches ($L=3$ in our experiments) and collect local preferences in a patch-wise way. With multiple dispreferred predictions, the objective of our LPO is as follows,

$$\mathcal{L}_{LPO}^{PL} = -\mathbb{E}_{\mathcal{D}_h} \left[\sum_{l=1}^{L^2} \log \sigma \left(-\log \sum_{j=1}^{J-1} \exp \left(\beta \log \frac{p_\theta(y_p^l | x^l)}{p_0(y_p^l | x^l)} - \beta \log \frac{p_\theta(y_{d_j}^l | x^l)}{p_0(y_{d_j}^l | x^l)} \right) \right) \right] \quad (8)$$

where $\{y_{d_j}^l\}_{j=1}^{J-1}$ is the set of dispreferred candidate predictions for the l th image patch x^l and y_p^l is the preferred local prediction.

2) **Sparse Local direct Preference Optimization (SLPO)**: While the proposed local preference learning can address the quality diversity of segmentation prediction in an image, it still requires substantial annotation efforts when the training set is large. It is harsh to expect the availability of human preferences on all patches. Thus, we further introduce SLPO, which requires local preferences on a small subset of patches within an image. Thus, the objective of our SLPO is as follows,

$$\mathcal{L}_{SLPO}^{PL} = -\mathbb{E}_{\mathcal{D}_h} \left[\sum_{l \in \mathcal{E}_d} \log \sigma \left(-\log \sum_{j=1}^{J-1} \exp \left(\beta \log \frac{p_\theta(\bar{y}_p^l | x^l)}{p_0(\bar{y}_p^l | x^l)} - \beta \log \frac{p_\theta(\bar{y}_{d_j}^l | x^l)}{p_0(\bar{y}_{d_j}^l | x^l)} \right) \right) \right] \quad (9)$$

where $\mathcal{E}_d \subset \{1, 2, \dots, L \times L\}$ contains the indexes of the labeled patches. By default, we use 15% of local patches in SLPO, which requires significantly reduced human annotation efforts.

3) **Candidate prediction generation**: In this study, we pair one preferred segmentation with multiple negatives in our preference data. While there are diverse ways to generate candidate segmentation predictions, we use a simple yet effective threshold-based strategy. Given a probabilistic prediction $p(x^t)$ for an input image x^t , we generate J binary segmentation predictions $\{y_j\}_{j=1}^J$ through a group of thresholds $\{\gamma_j\}_{j=1}^J$. The candidate predictions are further used to construct preference data in image-level way or local patch-level way.

F. Unsupervised Preference Learning

In this section, we further introduce Unsupervised direct Preference Optimization (UPO) with self-learned supervision

to address scenarios where no human preferences are available. For unsupervised and weakly supervised cross-domain segmentation, a typical segmentation defect in medical image segmentation is the imprecisely aligned boundary with the true object boundary, which may stem from the bias of the source domain annotations, domain gap, and ambiguity in object boundaries.

To address the issues of imprecise segmentation boundaries, we introduce self-learned pseudo label for the target domain. Specifically, given a coarse segmentation \hat{y}_0^t for a target training image x^t , we refine it with an edge-based active contour model, which evolves contours (e.g., the initial segmentation boundaries) to track the boundaries of desired objects under the guidance of an edge indicator g .

$$g \triangleq \frac{1}{1 + |\nabla G_\sigma * x^t|^2} \quad (10)$$

where G_σ is a gaussian kernel, σ determines the width of the gaussian kernel, $*$ is the convolution operation. For simplicity, we use a well-known level-set-based formulation, namely distance regularized level set evolution (DRLSE) [30], for the active contour model. Other more powerful methods [31]–[33] in variational formulation can also be used.

By applying active contour model on a coarse segmentation \hat{y}_0^t and we can obtain a refined segmentation \tilde{y}^t , which can be used to simulate a human rater through ranking the Dice scores between \tilde{y}^t and other candidate segmentation predictions. Thus, the preferred prediction is selected as follows,

$$y_p^t = \arg \max_{y \in \{y_j^t\}} \text{Dice}(\tilde{y}^t, y) \quad (11)$$

G. Overall Optimization

To train our domain-adaptive segmentation model, we incorporate the detection loss \mathcal{L}_{det} , segmentation loss \mathcal{L}_{seg} , contrastive learning loss \mathcal{L}_{pcl} , as well as the preference learning loss $\mathcal{L}_{\text{PO}}^{PL}$ with $\text{PO} \in \{\text{GPO}, \text{LPO}, \text{SLPO}, \text{UPO}\}$, depending on the availability of human preference data. The GPO refers to direct preference learning with global preference data, and UPO refers to unsupervised preference learning with the estimated preference data. The loss function for our Prefer-DAS model is as follows,

$$\mathcal{L}_{\text{Prefer-DAS}} = \mathcal{L}_{\text{seg}} + \lambda_1 \mathcal{L}_{\text{det}} + \lambda_2 \mathcal{L}_{\text{pcl}} + \lambda_3 \mathcal{L}_{\text{PO}}^{PL} \quad (12)$$

where λ_1 , λ_2 , and λ_3 are nonnegative tradeoff parameters. When $\lambda_3 = 0$, the Prefer-DAS model uses no preference learning and degenerates to the our preliminary conference version, i.e., Prompt-DAS. By default, our Prefer-DAS uses 15% points as training prompts, and our Prefer-DAS (SLPO) refers to the model using 15% training point prompts and human preferences on 15% local patches.

Significantly, the proposed model is a flexible framework and is capable of performing WDA, UDA, and Interactive Segmentation. Specifically, the Prefer-DAS model can conduct WDA when using sparse points, (sparse) human preferences, or both of them during model training. It can also conduct UDA without using sparse points and (sparse) human preferences, or with self-learned human preferences during

model training. Moreover, the Prefer-DAS model can conduct interactive segmentation when full/partial points are available during the inference stage.

V. EXPERIMENTS

A. Benchmark and Metrics

We evaluate the proposed method using four challenging datasets, where the images were scanned using different imaging technologies or taken from different tissues of different species.

Lucchi++. The Lucchi++ dataset [34] is a re-annotation of the EPFL Hippocampus dataset [35] by three neuroscience and biology experts. The EPFL Hippocampus data were taken from the CA hippocampus region of a mouse using Focused Ion Beam Scanning Electron Microscope (FIB-SEM) at a resolution of $5 \times 5 \times 5 \text{ nm}^3$. This dataset has two subsets of size $768 \times 1024 \times 165$ for training and testing, respectively.

MitoEM-Rat. The MitoEM-Rat dataset is a subset of MitoEM [36], acquired using multi-beam scanning electron microscopy (MB-SEM) at a resolution of $8 \times 8 \times 30 \text{ nm}^3$. The images in this dataset represent tissue taken from Layer II/III in the primary visual cortex of an adult mouse. The dataset contains a training subset of size $4096 \times 4096 \times 100$ and a testing subset of size $4096 \times 4096 \times 400$. This dataset features many large instances with complex morphologies and approximately 14.4k instances of mitochondria, significantly more than the Lucchi++ dataset.

MitoEM-Human. The MitoEM-Human dataset is a subset of MitoEM [36]. The MitoEM-Human data were introduced in [37] and was taken from the Layer II in the temporal lobe of an adult human using Multi-Beam Scanning Electron Microscopy (MB-SEM) at a resolution of $8 \times 8 \times 30 \text{ nm}^3$. The dataset contains a training subset of size $4096 \times 4096 \times 100$ and a testing subset of size $4096 \times 4096 \times 400$. Compared to the MitoEM-Rat dataset, MitoEM-Human contains a significantly higher number of instances of mitochondria, particularly small mitochondria. This variety in terms of shape and density makes the MitoEM-Human dataset a more challenging benchmark for analysis.

ME2-Stem. The ME2-Stem data were provided by Jiang et al. [38], and now this dataset is a subset of the MitoEM 2.0 Dataset. ME2-Stem data were taken from the brain stem of a mouse using Serial Block-Face Scanning Electron Microscopy (SBF-SEM) at a resolution of $8 \times 8 \times 30 \text{ nm}^3$. ME2-Stem data consist of mixed neural and glial populations. This dataset contains three $1000 \times 1000 \times 100$ -voxel volumes, designated for training, validation, and testing, respectively.

Adaptation Tasks. For model evaluation, we consider four cross-domain segmentation tasks: 1) from MitoEM-Human to MitoEM-Rat (**Human**→**Rat**), 2) from MitoEM-Rat to MitoEM-Human (**Rat**→**Human**), 3) from MitoEM-Human to Lucchi++ (**Human**→**Lucchi++**), and 4) from MitoEM-Human to ME2-Stem (**Human**→**Stem**). The four settings highlight the adaptation between datasets from different species and different tissues.

Evaluation metrics. Following [17], [22], we evaluate our method using the semantic-level Dice similarity coefficient

(Dice) and the instance-level Aggregated Jaccard Index (AJI) [39], as well as Panoptic Quality (PQ) [40].

B. Implementation Details

All the experiments are conducted on a single NVIDIA GeForce RTX 4090 GPU. We use DINO [41] as the backbone of our image encoder f_E and use the pretrained ViT-S/8 [41] to initialize the model parameters. Our decoder f_D follows a design similar to SAM, with the addition of masked self-attention and masked cross-attention mechanisms to prevent information leakage. In contrast to SAM, our prompt encoder employs standard positional embeddings. The MLP module is identical to that used in SAM and other standard Transformer architectures. In the training stage 1 (Prompt-DAS stage), the model is trained for 16k iterations with a batch size of 2 and an initial learning rate of 1×10^{-5} . For a fair comparison, the same data augmentations as those in WDA-Net [22] were used. Randomly cropped image patches of 384×384 were used for training. In the contrastive loss, we set $N^n=256$, $\delta_f=0.9$, $\delta_b=0.1$, and $\tau=0.5$. In the first stage, we set $\lambda_1=1e-3$, $\lambda_2=1e-3$, and $\lambda_3=0$ in the overall loss. In the training stage 2 (Preference Learning stage), the model is initialized from the student model obtained in the previous stage and fine-tuned for 16k iterations with a batch of 4 and an initial learning rate of 5×10^{-6} . In both stages, we optimize the model using the AdamW optimizer with a polynomial learning rate decay of power 0.9. We applied a group of 5 threshold values for candidate prediction generation: $\{0.3, 0.4, 0.5, 0.6, 0.7\}$. For the preference optimization loss, we use $\beta=1$ and $\sigma=1$. In this stage, we set $\lambda_1=0$, $\lambda_2=0$, and $\lambda_3=1$ in the overall loss.

C. Quantitative Comparison

To validate our method, we compare it with leading methods in both automatic and interactive segmentation modes. As shown in Table I, four settings of our models with different preference learning strategies are compared: Prompt-DAS, Prefer-DAS (UPO), Prefer-DAS (SLPO), and Prefer-DAS (LPO). The Prompt-DAS model is essentially Prefer-DAS without preference learning and was introduced in our preliminary conference paper [17]. Additionally, the Oracle model refers to the model that is trained on the target data with full pixel-wise labels.

Comparison with general/specialized foundation models. We begin by comparing our model with SAM [9], the well-known foundation segmentation model that is capable of operating in both automatic and interactive modes with instance-wise prompts, such as points and boxes. As demonstrated in Table I, the SAM model exhibits very low performance without model adaptation, primarily due to the significant differences between natural images and the EM images. While the SAM+ model, which utilizes a point prompt for each instance, shows improved results over SAM without interactions, its performance remains very low because of the shifted data distribution and the ambiguous boundaries of mitochondria in EM images. As shown in many studies [18], the SAM/SAM+ relies on sharp edges to delineate objects. Similar performance results are observed with the SAM-Med2D [11], which was

TABLE I

QUANTITATIVE COMPARISON. OUR PREFER-DAS IS COMPARED TO LEADING UDA, WDA, AND SAM-BASED APPROACHES IN BOTH AUTOMATIC AND INTERACTIVE SEGMENTATION MODES. THE PREFER-DAS MODEL IS FLEXIBLE TO CONDUCT BOTH UDA AND WDA, DEPENDING ON THE AVAILABILITY AND QUANTITY OF THE TRAINING POINT PROMPTS AND HUMAN PREFERENCES, AND CAN UTILIZE SPARSE POINT PROMPTS DURING INFERENCE. FOR INTERACTIVE SEGMENTATION, INDICATED BY A "+", FULL CENTER POINTS FOR ALL MITOCHONDRIA ARE USED AS TESTING PROMPTS TO FULFILL THE REQUIREMENTS OF SAM-LIKE METHODS. THE UPO, LPO, AND SLPO ARE THE PROPOSED UNSUPERVISED, LOCALLY SUPERVISED, AND SPARSE LOCALLY SUPERVISED PREFERENCE LEARNING. DICE (%), AJI (%), AND PQ (%) ARE USED AS MEASURES.

Types	Methods	Training Point Prompts	Human → Rat			Rat → Human			Human → Lucchi++			Human → Stem		
			Dice	AJI	PQ	Dice	AJI	PQ	Dice	AJI	PQ	Dice	AJI	PQ
Automatic Segmentation Mode														
NoAdapt	SAM [9]	0%	32.0	14.3	30.0	20.8	11.4	18.7	21.5	10.3	11.3	19.0	0.9	0.3
	SAM-Med2D [11]		15.9	-	-	22.5	-	-	23.1	12.7	2.6	27.9	13.0	3.3
	Med-SAM Adapter [12] [†]		75.5	56.6	27.5	72.4	55.0	33.4	64.6	44.8	19.5	27.8	12.9	7.1
	Prefer-DAS (Source)		88.6	76.7	68.7	78.1	62.8	55.5	85.6	73.5	66.8	76.8	45.3	45.8
UDA	UALR [5]	0%	86.3	71.6	53.7	83.8	69.7	60.0	81.3	68.1	63.2	65.5	38.7	28.7
	CAFA [7]		89.5	77.6	68.9	85.4	72.9	59.4	86.7	76.7	70.1	79.6	47.4	48.9
	DA-ISC [6]		88.6	75.7	65.8	85.6	72.7	63.8	85.2	72.8	64.1	72.0	38.8	35.6
	DAMT-Net [4]		88.7	76.3	61.8	85.4	72.3	63.7	86.6	75.5	73.0	78.6	48.0	53.5
	WDA-Net (UDA) [22]		88.2	74.5	59.0	85.5	72.3	60.6	85.6	74.3	71.9	74.5	48.2	44.0
	Prompt-DAS (UDA) [17]		92.4	82.2	74.3	88.0	76.6	68.1	87.3	76.9	73.1	82.9	51.6	53.6
	Prefer-DAS (UPO)		93.1	83.5	76.1	89.1	78.1	70.1	92.1	84.7	79.6	83.3	53.9	54.3
WDA	WDA-Net [22]	15%	91.7	80.7	74.0	88.7	77.6	67.8	86.3	75.6	70.8	80.7	48.8	50.0
	Prompt-DAS [17]		93.3	83.6	74.5	89.2	78.6	69.1	88.2	78.3	74.8	82.9	51.5	53.6
	Prefer-DAS (UPO)		93.7	84.4	77.5	90.1	80.1	71.2	92.6	85.6	80.9	83.4	51.9	53.8
	Prefer-DAS (SLPO)		94.3	85.5	79.1	91.8	82.8	74.7	93.2	86.8	81.3	84.2	63.7	59.7
	Prefer-DAS (LPO)		94.6	85.9	79.6	92.2	83.6	75.8	94.1	88.3	82.3	85.6	67.9	62.0
Interactive Segmentation Mode														
NoAdapt	SAM+	0%	40.6	1.2	26.2	40.3	4.6	26.6	81.1	68.1	67.6	39.0	12.6	15.4
	SAM-Med2D+		72.6	55.6	39.7	78.1	61.2	42.2	78.8	63.4	35.9	68.7	42.9	22.4
	Med-SAM Adapter+ [†]		86.2	70.2	59.9	83.8	68.1	59.0	86.8	74.0	56.8	49.7	9.6	18.2
	Prefer-DAS (Source)+		89.8	78.8	74.1	87.6	76.0	70.6	87.0	75.5	69.4	82.3	51.3	53.2
WDA	WeSAM+ [10] [‡]	15%	89.9	79.6	73.9	82.3	66.0	65.5	83.2	69.0	63.0	44.9	7.3	17.7
	Prompt-DAS+		93.5	84.4	74.2	90.8	81.5	72.3	88.7	79.1	74.8	83.8	52.0	53.6
	Prefer-DAS (UPO)+		94.3	85.4	79.2	90.9	81.2	71.6	93.4	87.1	82.5	84.2	52.5	53.9
	Prefer-DAS (SLPO)+		94.9	86.6	81.1	92.7	84.2	76.7	93.9	87.9	83.0	84.9	64.4	59.7
	Prefer-DAS (LPO)+		95.1	86.7	81.6	92.8	84.6	77.4	94.7	89.2	84.4	86.3	68.6	62.0
Segmentation Upper Bound														
Oracle	Fully-Supervised Model	-	94.6	86.4	79.2	92.6	84.6	75.8	95.1	90.1	85.8	84.8	71.9	71.9

[†] Fine-tuning using the source data

[‡] Fine-tuning using the source data and target data with 15% sparse point labels

trained by finetuning SAM with 4.6M medical images. When using full-point prompts, SAM-Med2D+ achieves substantial performance improvements—over 40% in Dice for all three tasks.

By finetuning the Medical SAM Adapter [12] on the EM images from the source domain (indicated with †), the Medical SAM Adapter[†] and its interactive version, Med-SAM Adapter+[†], demonstrate improved results for all four cross-domain segmentation tasks. However, these foundation models still exhibit a large performance gap compared to the supervised model, which represents the segmentation upper bound.

Additionally, the requirement of point prompts on all mitochondrion instances during inference is a limitation for practical use. In contrast, our Prefer-DAS model achieves strong performance with either no point prompts or just a few. When compared to the Oracle, our Prefer-DAS (LPO), without using any testing interaction, outperforms the supervised model by 0.8% in Dice on the Human→Stem task and shows only minor performance gaps of -0.3%, -0.8%, and

-1.9% in Dice on the other three domain-adaptation tasks, respectively, demonstrating its strong performance. With full point inference prompts, our Prefer-DAS+ model surpasses the supervised model in three of the four tasks, primarily due to the effective joint usage of the source and target data.

Comparison with UDA models. When using no label information on target training data, our Prefer-DAS model performs UDA segmentation and is referred to as **Prompt-DAS (UDA)**. Additionally, we denote **Prefer-DAS (UPO)** as our Prefer-DAS model that employs only unsupervised preference learning. As shown in Table I, our **Prefer-DAS** in the UDA mode, i.e., **Prompt-DAS (UDA)**, outperforms all other UDA methods, including various self-training based methods, WDA-Net (UDA) [22], UALR [5], and CAFA [7]. Integrating UPO to Prompt-DAS (UDA), our Prefer-DAS (UPO) model obtains a performance improvement of 0.7%, 1.1%, 4.2%, and 0.4% in Dice scores for the four respective tasks. Notably, larger performance gains are observed in terms of the AJI measure, indicating a better ability to correctly segment more mitochondria.

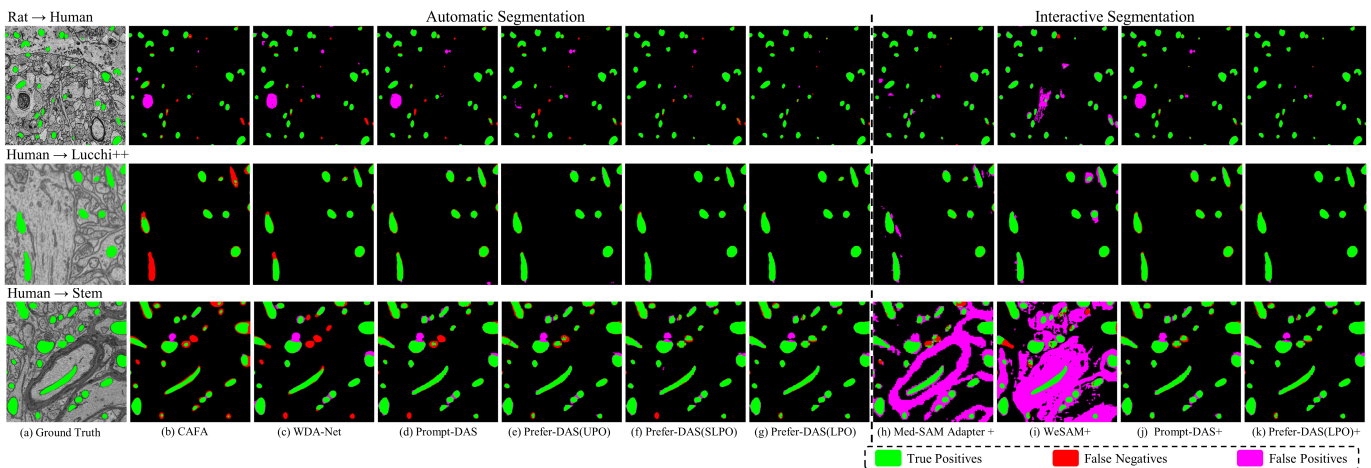


Fig. 3. Visual comparison of segmentation results in both automatic and interactive modes. Despite the Med-SAM Adapter+ and WeSAM+ being fine-tuned with the source EM data and utilizing full point prompts during inference, they still show severe false positive segmentation. In contrast, the proposed Prefer-DAS with LPO shows significantly reduced false positive and negative segmentation. With sparse local preferences on 15% patches, Prefer-DAS (SLPO) achieves comparable performance with Prefer-DAS (LPO).

Comparison with WDA models. Firstly, as shown in Table I, using 15% point labels as weak labels for training resulted in significant performance improvements for the WDA-Net, Prompt-DAS, and Prefer-DAS (UPO) models, particularly regarding instance-level AJI and PQ measures. Secondly, our Prefer-DAS (SLPO), which employs 15% sparse local preferences alongside 15% training point labels, outperforms all UDA and WDA methods that utilize 15% training point labels. Notably, our Prefer-DAS (SLPO) achieves impressive performance gains across all four tasks when compared to the WDA-Net and our Prompt-DAS, especially in terms of instance-level AJI and PQ measures. Even our Prefer-DAS (UPO), which relies solely on unsupervised preference learning, surpasses WDA-Net by substantial margins of 3.7%, 2.5%, 10.0%, and 3.1% in AJI for the four tasks, respectively. By using SLPO instead of UPO, Prefer-DAS (SLPO) demonstrates performance improvements of 1.1%, 2.7%, 1.2%, and 11.8% in AJI. Finally, using full local preferences, Prefer-DAS (LPO) obtains the best performance, showing significant performance improvements of 5.2%, 6.0%, 12.7%, and 19.1% in AJI over the WDA-Net. These results highlight the effectiveness of the proposed unsupervised preference learning and (sparse) local preference learning methodologies.

Finally, with testing prompts, our Prefer-DAS+ models can further obtain substantial performance improvements, and our Prefer-DAS(LPO)+ demonstrates the best performance among all the methods in comparison on all four tasks. Notably, in the interactive segmentation mode, our Prefer-DAS(LPO)+ even outperforms the supervised model on three of the four tasks, demonstrating the effectiveness of our method.

Visual comparison. Figure 3 presents a visual comparison of our proposed methods against several competing methods in both automatic and interactive modes. Overall, the qualitative comparison results highlight the superior performance of our Prefer-DAS model with significantly reduced false positives and false negatives in both modes. In contrast, the CAFA and Prompt-DAS exhibit a notable number of false negatives

for the Human \rightarrow Rat task and display more false positives for the Rat \rightarrow Human task. With unsupervised preference learning, Prefer-DAS (UPO) can effectively reduce false positives and negatives in large areas. Meanwhile, with supervised preference learning, Prefer-DAS (LPO) demonstrates the best visual performance, achieving minimal false positives and false negatives. Although using testing prompts can further enhance segmentation, the visual improvement is marginal, particularly when the original segmentation quality is already high.

D. Ablation Studies

Table II summarizes the results of ablation analysis conducted on the proposed model for two domain adaptation tasks. Specifically, we evaluate the contributions of several key components of our approach: 1) Detection Pseudo-labeling; 2) Segmentation Pseudo-labeling; 3) Using 15% sparse points as Training Prompts; 4) PCL: prompt-based contrastive learning; and 5) DPO: direct preference optimization.

For the DPO component, we compare four types of preference learning, 1) GPO: global direct preference optimization, which builds on image-level preference data; 2) LPO: the proposed local preference optimization that uses patch-level preference data; 3) SLPO: our 15% sparse local preference optimization that uses preference data on only a small proportion of local patches; and 4) UPO: the proposed unsupervised preference optimization, which relies on estimated segmentation as a substitute for human ratings.

As shown in Table II, the baseline Model I, i.e., our source model, can be improved by incorporating pseudo-labeling for detection or segmentation tasks. Through conducting multitask learning, Model IV outperforms Model I by 1.8%, 10.4%, and 3.8% in Dice scores for the three tasks, respectively. By using sparse points as training prompts, Model V achieves additional improvements of 2.3%, 0.4%, and 0.9% in Dice scores over Model IV for the three tasks. Furthermore, the integration of PCL into Model IV results in the creation of Prompt-DAS,

TABLE II

ABLATION STUDY OF OUR MODEL ON HUMAN → RAT, AND RAT → HUMAN. THE GPO, LPO, SLPO, AND UPO DENOTE PREFERENCE LEARNING USING IMAGE-LEVEL HUMAN PREFERENCES, PATCH-LEVEL HUMAN PREFERENCES, SPARSE PATCH-LEVEL PREFERENCES, AND SELF-LEARNED PREFERENCES. THE TRAINING PROMPTS DENOTE 15% SPARSE POINTS ON THE TARGET TRAINING DATA.

	Pseudo-labeling		Training Prompts	PCL	DPO				Human → Rat		Rat → Human	
	Detect.	Segment.			GPO	LPO	SLPO	UPO	Dice	PQ	Dice	PQ
Model I									88.6	68.7	78.1	55.5
Model II	✓								89.2	70.4	87.4	68.4
Model III		✓							89.5	70.0	87.7	68.3
Model IV	✓	✓							90.4	71.8	88.5	68.8
Model V	✓	✓	✓						92.7	74.1	88.9	69.0
Prompt-DAS	✓	✓	✓	✓					93.3	74.5	89.2	69.1
Prfer-DAS (GPO)	✓	✓	✓	✓	✓				94.3	78.7	91.5	74.2
Prfer-DAS (LPO)	✓	✓	✓	✓	✓	✓			94.6	79.6	92.2	75.8
Prfer-DAS (SLPO)	✓	✓	✓	✓	✓		✓		94.3	79.1	91.8	74.7
Prfer-DAS (UPO)	✓	✓	✓	✓	✓			✓	93.7	77.5	90.1	71.2

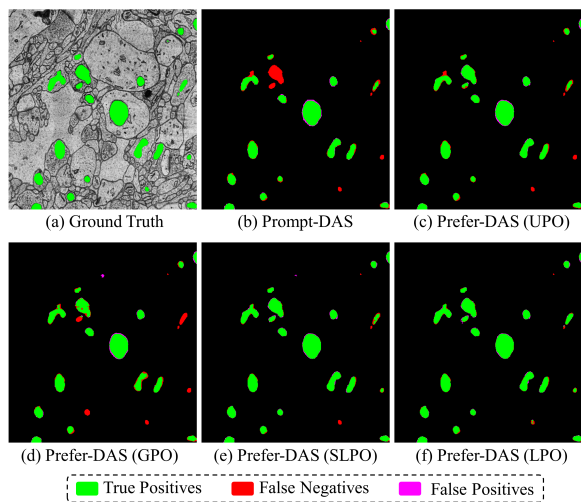


Fig. 4. Qualitative comparison of different strategies for preference learning. While UPO refers to learning using self-learned preferences, GPO and LPO refers to learning using image-level and patch-level human preferences, respectively. SLPO refers to using sparse LPO.

which leads to an average performance increase of 0.43% in Dice for all three tasks.

The lower half of the Table II demonstrates the performance of integrating various DPO strategies with Prompt-DAS. Overall, all DPO strategies significantly enhance segmentation performance, including the proposed unsupervised strategy. More specifically, the proposed LPO achieves the best segmentation performance across all three tasks. SLPO, the lightweight version of LPO, achieves similar performance with GPO in terms of Dice and PQ. Figure 4 presents a visual comparison of the Prefer-DAS with UPO, GPO, SLPO, and LPO. By integrating GPO to Prompt-DAS, the Prefer-DAS (GPO) reduces some false negatives but introduces new false negatives. In contrast, the LPO and SLPO rarely introduce new false negatives while rectifying existing segmentation errors.

E. Effectiveness of Local Preferences

In this section, we assess the effectiveness of using local preference data and multiple negatives in preference learning. Two DPOs for collecting and utilizing preference data are

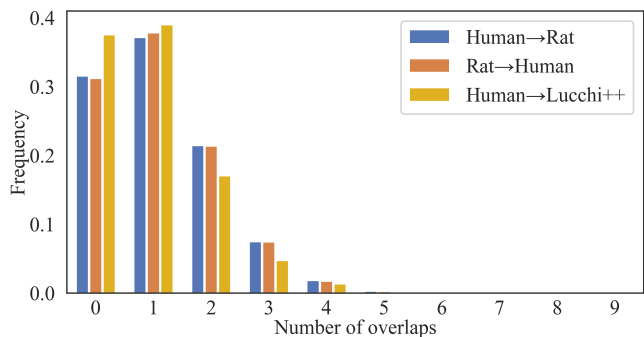


Fig. 5. Bar plot of the consistency between human preferences on the local patches and their whole image. For each image, we use 9 square patches of equal size. The frequency distributions on the training set of Rat, Human, and Lucchi++ data are shown.

compared: 1) GPO: the standard DPO that directly ranks candidate segmentation predictions at the image level, which poses significant challenges for human raters due to varying quality of segmentation across different sub-regions of each image; 2) LPO: the local DPO that ranks candidate predictions in a patch-wise way, offering more accurate and richer information about the segmentation quality. While giving global preference usually leads to inaccurate and inexact information about the segmentation quality, locally annotating preference allows for a focus on regions with poor segmentation quality.

Figure 5 illustrates the consistency between the preferences on local patches and its corresponding whole images. For over 30% images, the preferences at the image level completely differ from that on its patches. In approximately 60% of the images, the preferred segmentation at the image level aligns with only one or two of its nine patches, highlighting the necessity of utilizing local preferences.

Figure 6 presents a Box-and-Whisker plot of the Dice scores for both local and global preference learning, including UPO, GPO, LPO, and SLPO, across two domain-adaptation tasks. As shown in Fig. 6 our Prefer-DAS model with LPO outperforms the model with GPO by a large margin. These results confirm the effectiveness of local preference learning. Additionally, using preferences on only partial regions (15%),

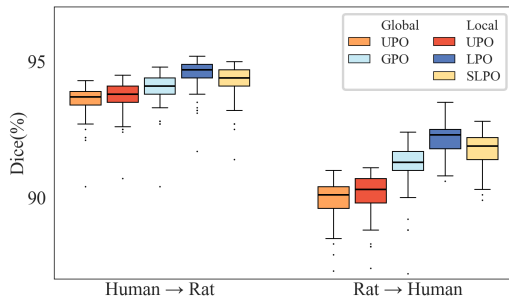


Fig. 6. Box-and-Whisker plot of the performance distributions of our Prefer-DAS using diverse local and global preference learning strategies. Global and local preferences refers to image-level and patch-level preferences, respectively.

TABLE III

ABLATION STUDY OF THE PREFER-DAS USING MULTIPLE NEGATIVES AND LOCAL PREFERENCES. THREE TASKS ARE USED FOR EVALUATION: HUMAN → RAT, RAT → HUMAN, AND HUMAN → LUCCHI++.

DPO	Negative(s)		Human → Rat		Rat → Human		Human → Lucchi++	
	Single	Multiple	Dice	PQ	Dice	PQ	Dice	PQ
GPO	✓		94.0	78.2	91.1	73.3	93.2	80.5
		✓	94.3	78.7	91.5	74.2	93.4	81.7
LPO	✓		94.2	78.0	91.3	74.7	93.9	82.3
		✓	94.6	79.6	92.2	75.8	94.1	82.3

the Prefer-DAS (SLPO) can even outperform the Prefer-DAS (GPO), demonstrating a good balance of model performance and annotation efficiency.

F. Impact of Multiple Negatives in Preference Learning

Table III summarizes the segmentation results using multiple negatives instead of a single negative in the preference data. As shown in Table III, the performance of using both LPO and GPO can be improved by using multiple negatives, which provides richer information about the dispreferred segmentation. Moreover, LPO with both single negative and multiple negatives shows improved performances over the GPO across all three tasks, validating the benefit of using local preference learning.

G. Effectiveness of Unsupervised Preference Learning

While the previous experiments have shown the effectiveness of supervised preference learning on reducing false positive and false negative segmentation, we further validate its effectiveness on correcting the other two types of segmentation errors: 1) incomplete mitochondria segmentation, as shown in the first row of Fig. 7; 2) misalignment of boundaries with target annotations, as shown in Fig. 7. While the incomplete segmentation mainly results from the domain gap, the boundary misalignment primarily arises from annotation differences between the source and target domains. Figure 7 illustrates typical examples of the Human → Lucchi++ task. Firstly, as shown in the first row of Fig. 7, the CAFA

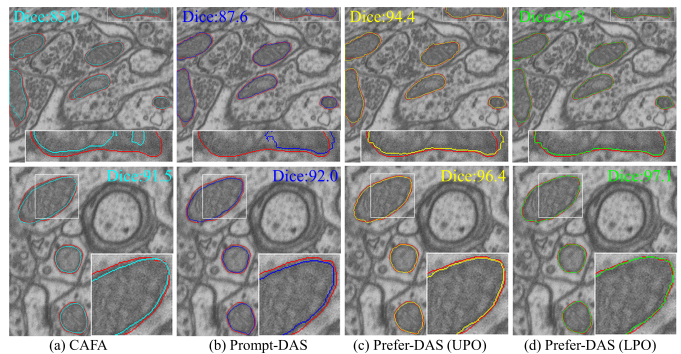


Fig. 7. Effectiveness of preference learning in correcting defective and biased segmentation. Red: Ground truth; Cyan: CAFA; Blue: Prompt-DAS, our model w/t preference learning; Yellow: Prefer-DAS (UPO); Green: Prefer-DAS (LPO). The Human → Lucchi++ task is used for evaluation. Both CAFA and Prompt-DAS reveal two types of segmentation defects: 1) incomplete mitochondria segmentation and 2) misalignment with target annotations. The misalignment primarily arises from the fact that the ground-truth annotations of the source and target domains align with the inner and outer membrane edges of the mitochondria, respectively.

TABLE IV

INFLUENCE OF THE QUANTITY OF TRAINING WEAK LABELS. BY DEFAULT, OUR PREFER-DAS (LPO) MODEL USES CENTER POINTS ON 15% MITOCHONDRIA AS TRAINING PROMPTS AND FULL LOCAL PREFERENCES. PREFER-DAS (SLPO) USES 15% POINTS AND 15% LOCAL PREFERENCES.

Training Labels		Human → Rat		Rat → Human		Human → Lucchi++	
Points	Preferences	Dice	PQ	Dice	PQ	Dice	PQ
0%	15%	94.3	78.7	91.7	74.3	92.8	80.4
15%	15%	94.3	79.1	91.8	74.7	93.2	81.3
100%	15%	94.4	79.1	92.0	75.4	94.0	82.9
15%	0%	93.7	77.5	90.1	71.2	92.6	80.9
15%	15%	94.3	79.1	91.8	74.7	93.2	81.3
15%	100%	94.6	79.6	92.2	75.8	94.1	82.3

model produces incomplete segmentation of four mitochondria, whereas the Prompt-DAS has incomplete segmentation of one mitochondrion. With UPO, the Prefer-DAS (UPO) shows significantly improved segmentation, but with smaller segmentation, which is corrected by using LPO. Secondly, the boundary misalignment between the predicted segmentation and the ground truth is more obvious in the second row of Fig. 7 due to the annotation bias on the source and target domains. Specifically, while the contours of ground truth annotations on MitoEM-Human data align with the inner membrane edges of mitochondria, the ground-truth contours of the Lucchi++ data align with the outer membrane edges of mitochondria. As shown in Fig. 7, both the CAFA method and our Prompt-DAS show biased segmentation similar to the source domain. Using unsupervised preference learning, our Prefer-DAS (UPO) shows significantly improved results. Moreover, learning with human preferences, the segmentation of the Prefer-DAS (LPO) model shows strong consistency with ground truth segmentation.

H. Influence of the Quantity of Training Weak Labels

A main goal of our study is to develop annotation-efficient method with sparse annotations. Significantly, our Prefer-DAS

model can take advantage of partial or full point annotations and local preferences and show strong performance with sparse annotations. To validate this, we conduct ablation studies on the annotation amounts of both point and local preference labels, which are summarized in Table IV. Obviously, using sparse annotations will substantially reduce annotation costs and the requirement of expert knowledge. For example, annotating points on a few mitochondria instances, which may be easily recognized by even non-experts, is significantly less challenging than annotating all instances. However, sparse annotations only provide reduced and incomplete knowledge about the target, posing significant challenges to developing segmentation models. From Table IV, we can observe that, although our model can show improved performance with more annotations, our Prefer-DAS with 15% point labels and 15% local preferences shows a good balance of annotation amount and model performance. Thus, we use 15% point labels and 15% local preferences by default, which results in our Prefer-DAS (SLPO) model.

I. Influence of the Quantity of Inference Point Prompts

Unlike the SAM, SAM-Med2D, Med-SAM Adapter, and WeSAM, our Prefer-DAS and Prompt-DAS can take advantage of both full points and partial points as prompts. Table V summarizes the comparison results of our models on three adaptation tasks using different proportions of point prompts for inference. Overall, using both full and partial points as inference prompts can improve the segmentation performance. Using 100% points for all instances can achieve the best results. However, assuming full points available during inference is prohibitive for processing large-scale EM stacks. As shown in Table V, using 15% or even 0% points, our models can achieve competitive performance on all three tasks while significantly reducing interaction requirements. Thus, our model shows wider applicability and can be applied to more scenarios with the availability of different amounts of interactions.

VI. CONCLUSION

This study presents Prefer-DAS, a novel framework that pioneers sparse promptable learning and (sparse) local human preference alignment for domain adaptive segmentation. Prefer-DAS allows for various configurations of utilizing points prompts and preferences, enabling it to perform UDA and WDA and perform both automatic and interactive segmentation during inference. To effectively utilize sparse point prompts, we develop a promptable multitask model that integrates self-training and prompt-guided contrastive learning. To address the dilemma between spatially varying preference alignment for semantic segmentation and image-level preference of DPO, we introduce local DPO, i.e., LPO, which is also flexible enough to use only sparse preferences on partial regions of a training image. Additionally, we introduce UPO, which conducts unsupervised preference learning. Comprehensive experiments conducted on four domain adaptation tasks demonstrate the effectiveness of our model across both UDA methods, WDA methods, and SAM-like methods at both

TABLE V
INFLUENCE OF THE QUANTITY OF INFERENCE POINT PROMPTS ON INTERACTIVE SEGMENTATION. WHILE SAM-LIKE METHODS REQUIRES FULL POINT PROMPTS FOR INTERACTIVE SEGMENTATION, THE PROPOSED PROMPT-DAS AND PREFER-DAS MODELS CAN TAKE ADVANTAGE OF PARTIAL POINT PROMPTS.

Model	Testing Prompts	Human→Rat		Rat→Human		Human→Lucchi++	
		Dice	PQ	Dice	PQ	Dice	PQ
Prompt-DAS	0%	93.3	74.5	89.2	69.1	88.2	73.7
	15%	93.5	74.2	90.0	69.8	88.6	74.7
	50%	93.5	74.2	90.4	70.9	88.6	74.8
	100%	93.5	74.2	90.8	72.3	88.7	74.8
Prefer-DAS (UPO)	0%	93.7	77.5	90.1	71.2	92.6	80.9
	15%	94.1	78.2	90.6	70.6	93.2	82.0
	50%	94.2	78.5	90.8	70.9	93.3	82.3
	100%	94.3	79.2	90.9	71.6	93.4	82.5
Prefer-DAS (SLPO)	0%	94.3	79.1	91.8	74.7	93.2	81.3
	15%	94.7	79.8	92.4	75.6	93.7	82.2
	50%	94.8	80.0	92.6	76.1	93.8	82.3
	100%	94.9	81.1	92.7	76.7	93.9	83.0
Prefer-DAS (LPO)	0%	94.6	79.6	92.2	75.8	94.1	82.3
	15%	94.9	80.3	92.7	76.5	94.5	83.5
	50%	95.0	80.6	92.8	76.8	94.6	84.0
	100%	95.1	81.6	92.8	77.4	94.7	84.4

automatic and interactive segmentation modes. In automatic segmentation mode, our model achieves performance that is close to or exceeds the supervised upper bound. In interactive mode, our model outperforms the supervised upper bound on three out of the four tasks.

One limitation of our method is that we have only considered one-step domain adaptation, which is challenging when new domains arrive continually. In future work, we will consider lightweight continuous domain adaptation with the method introduced in this study.

REFERENCES

- [1] K. Neikirk, E.-G. Lopez, A. G. Marshall, A. Alghanem, E. Krystofiak, B. Kula, N. Smith, J. Shao, P. Katti, and A. Hinton Jr, "Call to action to properly utilize electron microscopy to measure organelles to monitor disease," *European Journal of Cell Biology*, vol. 102, no. 4, p. 151365, 2023.
- [2] O. Ronneberger, P. Fischer, and T. Brox, "U-net: Convolutional networks for biomedical image segmentation," in *International Conference on Medical Image Computing and Computer-Assisted Intervention*, 2015, pp. 234–241.
- [3] A. Dosovitskiy, L. Beyer, A. Kolesnikov, D. Weissenborn, X. Zhai, T. Unterthiner, M. Dehghani, M. Minderer, G. Heigold, S. Gelly, J. Uszkoreit, and N. Houlsby, "An image is worth 16x16 words: Transformers for image recognition at scale," in *International Conference on Learning Representations*, 2021.
- [4] J. Peng, J. Yi, and Z. Yuan, "Unsupervised mitochondria segmentation in em images via domain adaptive multi-task learning," *IEEE Journal of Selected Topics in Signal Processing*, vol. 14, no. 6, pp. 1199–1209, 2020.
- [5] S. Wu, C. Chen, Z. Xiong, X. Chen, and X. Sun, "Uncertainty-aware label rectification for domain adaptive mitochondria segmentation," in *International Conference on Medical Image Computing and Computer Assisted Intervention*, 2021, pp. 191–200.
- [6] W. Huang, X. Liu, Z. Cheng, Y. Zhang, and Z. Xiong, "Domain adaptive mitochondria segmentation via enforcing inter-section consistency," in *International Conference on Medical Image Computing and Computer Assisted Intervention*, 2022, pp. 89–98.

- [7] D. Yin, W. Huang, Z. Xiong, and X. Chen, "Class-aware feature alignment for domain adaptive mitochondria segmentation," in *International Conference on Medical Image Computing and Computer-Assisted Intervention*, 2023, pp. 238–248.
- [8] D. Qiu, J. Yi, and J. Peng, "Wda-net: Weakly-supervised domain adaptive segmentation of electron microscopy," in *IEEE International Conference on Bioinformatics and Biomedicine*, 2022, pp. 1132–1137.
- [9] A. Kirillov, E. Mintun, N. Ravi, H. Mao, C. Rolland, L. Gustafson, T. Xiao, S. Whitehead, A. C. Berg, W.-Y. Lo *et al.*, "Segment anything," in *Proceedings of the IEEE/CVF International Conference on Computer Vision*, 2023, pp. 4015–4026.
- [10] H. Zhang, Y. Su, X. Xu, and K. Jia, "Improving the generalization of segmentation foundation model under distribution shift via weakly supervised adaptation," in *Proceedings of the IEEE/CVF Conference on Computer Vision and Pattern Recognition*, 2024, pp. 23 385–23 395.
- [11] J. Cheng, J. Ye, Z. Deng, J. Chen, T. Li, H. Wang, Y. Su, Z. Huang, J. Chen, L. Jiang *et al.*, "Sam-med2d," *arXiv preprint arXiv:2308.16184*, 2023.
- [12] J. Wu, W. Ji, Y. Liu, H. Fu, M. Xu, Y. Xu, and Y. Jin, "Medical sam adapter: Adapting segment anything model for medical image segmentation," *arXiv preprint arXiv:2304.12620*, 2023.
- [13] P. F. Christiano, J. Leike, T. Brown, M. Martic, S. Legg, and D. Amodei, "Deep reinforcement learning from human preferences," *Advances in Neural Information Processing Systems*, vol. 30, 2017.
- [14] R. Rafailov, A. Sharma, E. Mitchell, C. D. Manning, S. Ermon, and C. Finn, "Direct preference optimization: Your language model is secretly a reward model," *Advances in Neural Information Processing Systems*, vol. 36, pp. 53 728–53 741, 2023.
- [15] B. Wallace, M. Dang, R. Rafailov, L. Zhou, A. Lou, S. Purushwalkam, S. Ermon, C. Xiong, S. Joty, and N. Naik, "Diffusion model alignment using direct preference optimization," in *Proceedings of the IEEE/CVF Conference on Computer Vision and Pattern Recognition*, 2024, pp. 8228–8238.
- [16] S. Li, K. Kallidromitis, A. Gokul, Y. Kato, and K. Kozuka, "Aligning diffusion models by optimizing human utility," *Advances in Neural Information Processing Systems*, vol. 37, pp. 24 897–24 925, 2024.
- [17] J. Chen, S. Xiong, and J. Peng, "Prompt-das: Annotation-efficient prompt learning for domain adaptive semantic segmentation of electron microscopy images," in *International Conference on Medical Image Computing and Computer-Assisted Intervention*. Springer, 2025, pp. 512–521.
- [18] M. Ali, T. Wu, H. Hu, Q. Luo, D. Xu, W. Zheng, N. Jin, C. Yang, and J. Yao, "A review of the segment anything model (sam) for medical image analysis: Accomplishments and perspectives," *Computerized Medical Imaging and Graphics*, vol. 119, p. 102473, 2025.
- [19] J. Hoffman, E. Tzeng, T. Park, J.-Y. Zhu, P. Isola, K. Saenko, A. Efros, and T. Darrell, "Cycada: Cycle-consistent adversarial domain adaptation," in *International Conference on Machine Learning*. Pmlr, 2018, pp. 1989–1998.
- [20] Y. Ganin, E. Ustinova, H. Ajakan, P. Germain, H. Larochelle, F. Laviolette, M. March, and V. Lempitsky, "Domain-adversarial training of neural networks," *Journal of Machine Learning Research*, vol. 17, no. 59, pp. 1–35, 2016.
- [21] Y. Tsai, W. Hung, S. Schuster, K. Sohn, M. Yang, and M. Chandraker, "Learning to adapt structured output space for semantic segmentation," in *IEEE Conference on Computer Vision and Pattern Recognition*, 2018, pp. 7472–7481.
- [22] D. Qiu, S. Xiong, J. Yi, and J. Peng, "Weakly-supervised cross-domain segmentation of electron microscopy with sparse point annotation," *IEEE Transactions on Big Data*, vol. 11, no. 2, pp. 359–371, 2025.
- [23] R. A. Bradley and M. E. Terry, "Rank analysis of incomplete block designs: I. the method of paired comparisons," *Biometrika*, vol. 39, no. 3/4, pp. 324–345, 1952.
- [24] Y. Chen, J. Tan, A. Zhang, Z. Yang, L. Sheng, E. Zhang, X. Wang, and T.-S. Chua, "On softmax direct preference optimization for recommendation," *Advances in Neural Information Processing Systems*, vol. 37, pp. 27 463–27 489, 2024.
- [25] R. L. Plackett, "The analysis of permutations," *Journal of the Royal Statistical Society Series C: Applied Statistics*, vol. 24, no. 2, pp. 193–202, 1975.
- [26] L. Zhu, T. Chen, Q. Xu, X. Liu, D. Ji, H. Wu, D. W. Soh, and J. Liu, "Popen: Preference-based optimization and ensemble for lvlm-based reasoning segmentation," in *Proceedings of the Computer Vision and Pattern Recognition*, 2025, pp. 30 231–30 240.
- [27] A. Konwer, Z. Yang, E. Bas, C. Xiao, P. Prasanna, P. Bhatia, and T. Kass-Hout, "Enhancing sam with efficient prompting and preference optimization for semi-supervised medical image segmentation," in *Proceedings of the Computer Vision and Pattern Recognition*, 2025, pp. 20 990–21 000.
- [28] A. Tarvainen and H. Valpola, "Mean teachers are better role models: Weight-averaged consistency targets improve semi-supervised deep learning results," in *Advances in Neural Information Processing Systems*, vol. 30, 2017.
- [29] F. Li, H. Zhang, S. Liu, J. Guo, L. M. Ni, and L. Zhang, "Dn-detr: Accelerate detr training by introducing query denoising," in *Proceedings of the IEEE/CVF Conference on Computer Vision and Pattern Recognition*, 2022, pp. 13 619–13 627.
- [30] C. Li, C. Xu, C. Gui, and M. D. Fox, "Distance regularized level set evolution and its application to image segmentation," *IEEE Transactions on Image Processing*, vol. 19, no. 12, pp. 3243–3254, 2010.
- [31] P. Hu, F. Wu, J. Peng, P. Liang, and D. Kong, "Automatic 3d liver segmentation based on deep learning and globally optimized surface evolution," *Physics in Medicine & Biology*, vol. 61, no. 24, p. 8676, 2016.
- [32] P. Hu, F. Wu, J. Peng, Y. Bao, F. Chen, and D. Kong, "Automatic abdominal multi-organ segmentation using deep convolutional neural network and time-implicit level sets," *International Journal of Computer Assisted Radiology and Surgery*, vol. 12, no. 3, pp. 399–411, 2017.
- [33] J. Peng, P. Hu, F. Lu, Z. Peng, D. Kong, and H. Zhang, "3d liver segmentation using multiple region appearances and graph cuts," *Medical Physics*, vol. 42, no. 12, pp. 6840–6852, 2015.
- [34] V. Casser, K. Kang, H. Pfister, and D. Haehn, "Fast mitochondria segmentation for connectomics," in *Proceedings of Machine Learning Research*, 2020, pp. 111–120.
- [35] A. Lucchi, K. Smith, R. Achanta, G. Knott, and P. Fua, "Supervoxel-based segmentation of mitochondria in em image stacks with learned shape features," *IEEE Transactions on Medical Imaging*, vol. 31, no. 2, pp. 474–486, 2011.
- [36] D. Wei, Z. Lin, D. Franco-Barranco, N. Wendt, X. Liu, W. Yin, X. Huang, A. Gupta, W.-D. Jang, X. Wang *et al.*, "Mitoem dataset: Large-scale 3d mitochondria instance segmentation from em images," in *International Conference on Medical Image Computing and Computer-Assisted Intervention*, 2020, pp. 66–76.
- [37] A. Shapson-Coe, M. Januszewski, D. R. Berger, A. Pope, Y. Wu, T. Blakely, R. L. Schalek, P. H. Li, S. Wang, J. Maitin-Shepard *et al.*, "A connectomic study of a petascale fragment of human cerebral cortex," *BioRxiv*, pp. 2021–05, 2021.
- [38] Y. Jiang, H. Wang, K. M. Boergens, N. Rzepka, F. Wang, and Y. Hua, "Efficient cell-wide mapping of mitochondria in electron microscopic volumes using webknossos," *Cell Reports Methods*, vol. 5, no. 2, 2025.
- [39] N. Kumar, R. Verma, S. Sharma, S. Bhargava, A. Vahadane, and A. Sethi, "A dataset and a technique for generalized nuclear segmentation for computational pathology," *IEEE Transactions on Medical Imaging*, vol. 36, no. 7, pp. 1550–1560, 2017.
- [40] A. Kirillov, K. He, R. Girshick, C. Rother, and P. Dollar, "Panoptic segmentation," in *Proceedings of the IEEE/CVF Conference on Computer Vision and Pattern Recognition*, 2019, pp. 9404–9413.
- [41] M. Caron, H. Touvron, I. Misra, H. Jégou, J. Mairal, P. Bojanowski, and A. Joulin, "Emerging properties in self-supervised vision transformers," in *Proceedings of the IEEE/CVF International Conference on Computer Vision*, 2021, pp. 9650–9660.